Article:
Wang, C., Li, Z., Sheng, B. et al. (2024) A Twisting Mechanism With Parallel Springs for Series Variable Stiffness Actuator. IEEE/ASME Transactions on Mechatronics. ISSN: 1083-4435

https://doi.org/10.1109/tmech.2024.3378740

A Twisting Mechanism with Parallel Springs for Series Variable Stiffness Actuator

Chao Wang, Zhenhong Li, *Member, IEEE*, Bo Sheng, *Member, IEEE*, Tianzhe Bao, Manoj Sivan, Zhi-Qiang Zhang, *Member, IEEE*, Sheng Quan Xie, *Senior Member, IEEE*, and Gu-Qiang Li

***Abstract*—This paper proposes a novel twisting mechanism with parallel springs (TPS) employing eight parallel springs in 3D configuration and a ball screw mechanism to achieve space-efficient stiffness regulation. Based on TPS, a compact VSA prototype, named TPS-VSA, is developed. Two models are established to estimate the output torque of the actuator based on deflection angles and angular speed. One is a conventional model derived from the mechanical structure, and the other is a 6-degree polynomial model fitted with experimental data. Simulation and experiment studies are conducted to evaluate the torque and stiffness regulation property of TPS-VSA, and the performance of the torque estimation models. The experimental results show that the proposed mechanism is effective in varying the stiffness of VSAs. Both the polynomial and conventional models performed well for estimating the output torque of the TPS-VSA, but the polynomial model has an average error of less than 0.0737 Nm, which significantly outperforms the conventional model (which has an average error above 0.1167 Nm). The dynamic behavior and frequency responses obtained through free vibration test shows that the natural frequency of TPS-VSA can be effectively changed by the proposed mechanism. The result of stiffness regulation test demonstrates that TPS-VSA can achieve the whole range stiffness variation within 0.9 s. The result of trajectory tracking test indicates that TPS-VSA can accurately track different trajectories with a simple PID controller.**

***Index Terms*—Physical Human-Robot Interaction, Series Elastic Actuator, Variable Stiffness.**

I. INTRODUCTION

Many compliant robotic actuators have been developed for safe physical human-robot interaction (pHRI) [1], [2], e.g., series elastic actuators (SEAs) [3] and parallel elastic actuators (PEAs) [4]–[6]. Most of the actuators are developed with fixed stiffness based on a preset working environment. However, the growing intricacy of pHRI necessitates the adjustable stiffness of actuators to enhance its adaptability and resilience. Impedance control has been developed to emulate variable stiffness behaviors based on force/torque feedback [7]. It has indeed made significant advancements in pHRI. Nonetheless, it is essential to recognize that this approach may not guarantee a robust interaction under all circumstances. One critical concern is the system's vulnerability in the event of sensor failure, where the reliance on force and torque feedback becomes a potential weakness [2], [8]. Additionally, by introducing elastic element, the output torque/force of compliant actuators can be estimated without force/torque sensors, reducing the size, and cost [9], [10].

Depending on the structure, VSAs can be grouped into three types, i.e., antagonistic-type [11]–[13], parallel-type [14], [15], and series-type [16]–[18]. Antagonistic-type VSAs work similarly to the human musculoskeletal system, using two opposing operators to adjust stiffness and output torque. This principle enables easy compensation of potential misalignment between the joint and actuator, which is a typical issue in cable-driven robotic systems [19]. Nevertheless, only one motor can contribute to the maximal output capacity, and energy storage from one spring if the actuator is not bidirectional limiting the energy efficiency [19]. Additionally, the range of stiffness

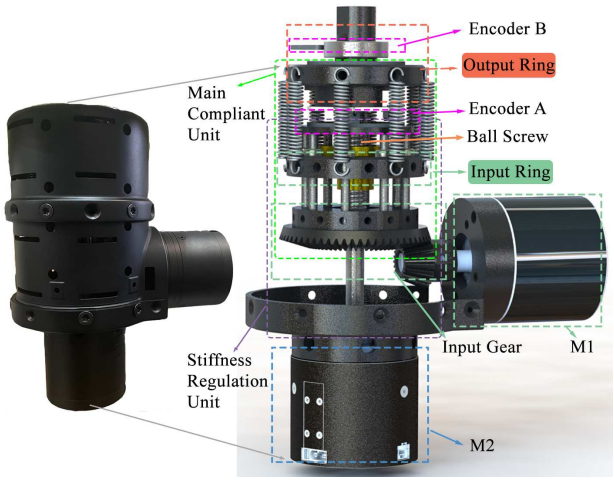

Fig. 1. Prototype (left) and structure (right) of the proposed VSA. DC motors, M1 and M2, control the output ring and spring preload, respectively. Encoder A captures the deflection between the input and output rings. Encoder B monitors the displacement of output ring.

This work is conducted in the Institute of Rehabilitation Engineering, Binzhou Medical University, Yantai, 264033, China. This work was supported in part by U.K. EPSRC under Grant EP/V057782/1 and EP/S019219/1, and the Shanghai Pujiang Program, under Grant 21PJ1404000, and the National Natural Science Foundation of China, under Grant 62103252. (*Corresponding authors: Sheng Quan Xie, Gu Qiang Li, Bo Sheng.*)

Chao Wang and Zhi Qiang Zhang are with the School of Electrical and Electronic Engineering, University of Leeds, Leeds, LS2 9JT, U.K. (e-mail: elcw@leeds.ac.uk, z.zhang3@leeds.ac.uk).

Zhenhong Li is with the Department of Electrical & Electronic Engineering, University of Manchester, Manchester, M13 9PL, U.K. (e-mail: zhenhong.li@manchester.ac.uk).

Bo Sheng is with the School of Mechatronic Engineering and Automation, Shanghai University, 99 Shangda Road, Baoshan District, 20044, Shanghai, China (e-mail: shengbo@shu.edu.cn).

Tianzhe Bao is with the Institute of Rehabilitation Engineering, University of Health and Rehabilitation Science, Qingdao 261000, China (e-mail: tianzhe.bao@uor.edu.cn)

Manoj Sivan is with the Academic Department of Rehabilitation Medicine, University of Leeds, Leeds, LS2 9JT, U.K. (e-mail: m.sivan@leeds.ac.uk).

Gu Qiang Li is with the Institute of Rehabilitation Engineering, Binzhou Medical University, Yantai 264033, China (e-mail: lgq100@bzmc.edu.cn).

Sheng Quan Xie collaborates with the Institute of Rehabilitation Engineering, Binzhou Medical University, Yantai 264033, China, he is with the School of Electronic and Electrical Engineering, University of Leeds, Leeds LS2 9JT, U.K. (e-mail: s.q.xie@leeds.ac.uk).

adjustment is determined by the motor with lower power, which imposes constrains on the selection of suitable motors. Parallel-type VSAs consist of an actuator in parallel with one or more elastic elements such as springs working together. However, the lower boundary of the stiffness adjustment is limited due to the parallel structure [14]. Series-type VSAs use two independent operators for output torque and stiffness regulation. This feature facilitate a better motor selection to precisely match required power, thus reducing size and weight.

Stiffness variation principles employed in series-type VSAs design can be categorized as follows: 1) changing transmission ratio, 2) changing property of elastic elements, and 3) changing preload of elastic elements. The principle of changing transmission ratio achieves stiffness regulation by adjusting the effective length or position of the transmission components. For example, the SVSA-II integrates symmetrical stiffness transmission mechanism with two adjustable pivot lever arms driven by Archimedean spiral gear [20], while this design introduces a significant friction to the force transmission system. Similarly, the CompAct-VSA employs a gear-rack and a cam mechanism to adjust the pivot point [21]. There are also many other typical VSAs based on the same principle including AwAS-II [16], [17], VSSEA [18], and [22]. However, the transmission ratio adjustment mechanisms are bulky, complex, and potentially less efficient in regulating stiffness. Alternatively, there are actuators modifying the properties of elastic elements to adjust stiffness. They achieve this by manipulating the characteristics of the materials or changing the structures used as compliant components. Examples of such actuators include S^3VSA [24], [25], and [31]. Similarly, the fluid-based actuators changes the status of fluid to regulate the stiffness, e.g., pneumatic [26]–[28], hydraulic [29], [30], and also the magnetorheological actuators [39]–[41]. These actuators normally have a high power-to-weight ratio, while the high non-linear characteristic brings big challenges to control. The principle of changing preload adjusts the stiffness by modifying the initial deformation of elastic elements using independent mechanisms and motor, and the structure of these actuators is simple and easy to control, e.g., MACCEPA 2.0 [23], LVSA [9], and the recently proposed various reconfigurable actuators [10], [24], [32].

Early studies simplified the dynamics of both antagonistic-type and series-type actuators as planar models since both force and moment arm vectors reside in two parallel planes [9], [32]–[37]. Consequently, these actuators require additional transmission mechanisms, e.g., linkages and belt, in the design to ensure that the dynamics model matches the mechanical structure better, which limits the optimization of structure, and size of the actuator.

This study proposes a novel twisting mechanism for stiffness regulation by expanding the force and moment arm of elastic elements to three dimensional space. A VSA is designed by on the proposed mechanism, whose output torque and stiffness are controlled by two independent DC motors, see Fig. 1. A ball screw mechanism is employed to adjust the distance between the two rings, thereby the preload of springs can be changed to regulate the stiffness. The main contributions of this paper are threefold.

1) A twisting mechanism with parallel springs, TPS, is proposed for stiffness variation of SEAs. In comparison with the VSA mechanisms proposed in previous studies, the presented mechanism is distributed in a three-dimensional space, offering advantages in terms of structure and size optimization. Moreover, the TPS mechanism provides a larger tolerance for safe pHRI compared to irregular springs. Importantly, it directly couples the input and output rings, enhancing energy efficiency in contrast to indirect methods such as a cam mechanism.
2) A torque estimation approach based on polynomial model is established to estimate the output torque of the VSA based on the deflection angles and its change rate. By comparison, a torque estimation model based on the mechanical structure of the proposed VSA is established to estimate the output torque as well.
3) A prototype of the proposed VSA is created to evaluate the torque estimation accuracy of the proposed method, stiffness regulation speed, and dynamic behavior. Then, a position tracking test is demonstrated with the prototype.

The remaining paper is organized as follows: Section II introduces the TPS mechanism and stiffness variation principle of the proposed VSA. Section III establishes the torque-deflection and stiffness-deflection relationships, including a conventional and polynomial model for output torque estimation. Experiments setup of performance test is described in IV. Performance test result is presented and discussed in Section V, and VI, respectively. Section VII concludes this paper.

II. DESIGN

A. Working Principle

VSAs based on planar models can be simplified as Fig. 2 (a) [9], [10], [16], [23], [32]. This structure requires the VSA leave enough space for the output ring and the elastic element. As a result, the dimensions of the actuator along this direction need to be bigger to increase the range of stiffness adjustment and output torque.

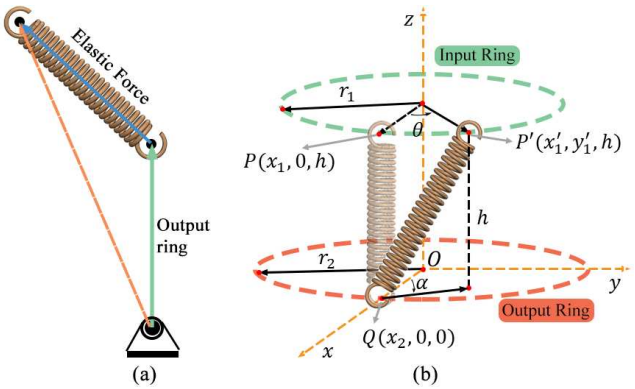

Fig. 2. (a) Working principle of the VSAs based on the planar models. (b) Working principle of one branch of TPS mechanism: θ is the deflection angle between the input and output rings; P is the initial position of the coupling point between spring and input ring, P' is the position of the coupling point when deflection angle between the two rings is θ; O is the central position of output ring; Q is the position of the coupling point between the output ring and the spring; r_1, and r_2 are the radius of input and output rings, respectively; h is the distance between the two rings.

In this study, a mechanism, TPS, is proposed for stiffness variation of SEAs, see Fig. 2 (b). There are two rings in TPS mechanism, i.e., input and output rings, coupled through springs. The projection of spring force on the output ring is along the radial direction of the ring at the initial position, denoted as P, implying zero output torque. The spring force produces torque along the z-axis with the passive movement of output ring, and the value of the output torque is related to deflection angle θ, distance between the two rings h, and spring stiffness k_s. Variation of h changes preload of springs which determines the output stiffness. Besides, the stiffness can also be adjusted by reconfiguring the number and inherent stiffness of the springs.

B. Mechanical Structure

The design of TPS-VSA is shown in Fig. 1. The actuator has two units: main driver and stiffness adjuster. The main driver controls the output torque, rotational speed and position of the VSA via regulating θ. The stiffness adjuster regulates the distance h and change the preload of springs. The position of the input gear is fixed. As shown in Fig. 3, the ball screw nut is rigidly fixed to the input ring, and the nut will rotate along with the input ring. This will induce a change in h. The input gear is rigidly connected with eight bars (linear slider rail) which is coupled with the input ring through eight linear sliders. Therefore, the rotation of the ball screw changes the position of the input ring along the z-axis, and the deflection of input gear drive causes the same deflection on the input ring. Consequently, the rotary motion and the displacement along the z-axis of the input ring (stiffness regulation) is decoupled.

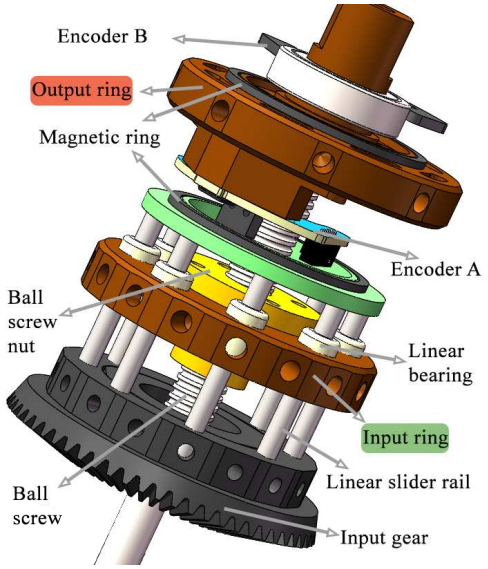

Fig. 3. The structure of the main driver and the connection between the input gear and input ring.

The magnetic ring is immovably connected with the eight bars, thereby the input gear, the eight bars and the magnetic ring is considered as a rigid body. The encoder A is fixedly joined with the output ring to measure the deflection angle between the magnetic ring and output ring which reflects the deflection angle between the input and output rings θ in Fig. 2 (b). The encoder B is fixed on the external cased of the TPS-VSA to capture the output ring deflection angle related to the case, which is defined as γ. The displacement of the input ring along the z-axis is controlled by M2 through the ball screw which is rigidly joined with M2. Thereby, the deflection angle of the ball screw is considered as the same as M2. The magnetic encoder in M2 is used to measure the ball screw shaft deflection angle and calculate the distance between input and output rings, i.e., h in Fig. 2 (b).

III. METHODOLOGY

A. Stiffness Modeling

To model the stiffness and estimate output torque of the TPS-VSA, the following assumptions are made.

Assumption 1. *All the components of TPS-VSA are considered as rigid except the elastic elements.*

Assumption 2. *The two ends of every elastic element are rigidly connected with the two rings, respectively.*

The kinematics of the system can be formulated as:

$$\begin{aligned} \cos\alpha &= \frac{x_1' - x_2}{\sqrt{(x_1' - x_2)^2 + y_1'^2}} \\ x_1' &= r_1\cos\theta \\ y_1' &= r_1\sin\theta. \end{aligned} \tag{1}$$

Let the angle between $\overrightarrow{QP'}$ and the xOy plane be β, the following can be found

$$\sin\beta = \frac{h}{\sqrt{(r_1\cos\theta - r_2)^2 + (r_1\sin\theta)^2 + h^2}}. \tag{2}$$

Let the original length of the springs and the minimal distance between the two rings be l_0, and h_{min} ($h_{min} \geq l_0$), respectively. The spring stretched length can be obtained by

$$\Delta l = \sqrt{(r_1\cos\theta - r_2)^2 + (r_1\sin\theta)^2 + h^2} - l_0. \tag{3}$$

Then, the spring force can calculated as

$$F_s = k_s\Delta l \tag{4}$$

where F_s is the force produced by a single spring, k_s is the stiffness of one springs, h can be obtained by

$$h = h_0 + \Delta h_1 + \Delta h_2 \tag{5}$$

where h_0 is the initial value of h, Δh_1, and Δh_2 are the change of h contributed by θ and rotation of M2 λ, respectively, which can be computed by

$$\begin{aligned} \Delta h_1 &= \frac{\theta}{2\pi}d \\ \Delta h_2 &= \frac{\lambda}{2\pi}d \end{aligned} \tag{6}$$

where d is the lead length of the ball screw.

The output torque of the actuator can be computed by

$$\tau = NF_{xy}r \tag{7}$$

where F_{xy} is the projection of the spring force on the xOy plane, N is the number of springs, and r is the moment arm of F_{xy}, which can be calculated by

$$\begin{aligned} r &= r_2 \sin\alpha \\ &= \frac{r_1 r_2 \sin\theta}{\sqrt{(r_1\cos\theta - r_2)^2 + (r_1\sin\theta)^2}} \end{aligned} \tag{8}$$

and F_{xy} can be calculated by

$$\begin{aligned} F_{xy} &= F_s \cos\beta \\ &= \frac{k_s \Delta l \sqrt{(r_1\cos\theta - r_2)^2 + (r_1\sin\theta)^2}}{\sqrt{(r_1\cos\theta - r_2)^2 + (r_1\sin\theta)^2 + h^2}}. \end{aligned} \tag{9}$$

The equivalent stiffness of the actuator is defined as

$$\begin{aligned} k_{eq} &= \frac{\delta\tau}{\delta\theta} \\ &= r\frac{\delta F_{xy}}{\delta\theta} + F_{xy}\frac{\delta r}{\delta\theta} \\ &= N\delta_l k s r_1 r_2 \\ &\frac{\left(-r_1^2\sin(\theta)\cos(\theta) + r_1(r_1\cos(\theta) - r_2)\sin(\theta)\right)\sin(\theta)}{\left(h^2 + r_1^2\sin^2(\theta) + (r_1\cos(\theta) - r_2)^2\right)^{\frac{3}{2}}} \\ &+ \frac{N\delta_l k s r_1 r_2 \cos(\theta)}{\sqrt{h^2 + r_1^2\sin^2(\theta) + (r_1\cos(\theta) - r_2)^2}}. \end{aligned} \tag{10}$$

B. Elastic Element Reconfiguration

By reconfiguring the material, size, and number of the elastic elements, the upper and lower boundary of the stiffness range of the actuator can be adjusted, making the VSA adaptable to different working conditions. Theoretically, the proposed VSA can achieve a stiffness range from zero to rigid if the input and output rings are coupled through rigid bars. In this study, the actuator is tested with spring stiffness $k_s =$ 3300 N/m. Fig. 4 illustrates the stiffness-deflection and torque-deflection relations for $k_s = 3300$ N/m, based on Eqns. (7), and (10), respectively. k_s is calculated based on the material and dimensions of the spring.

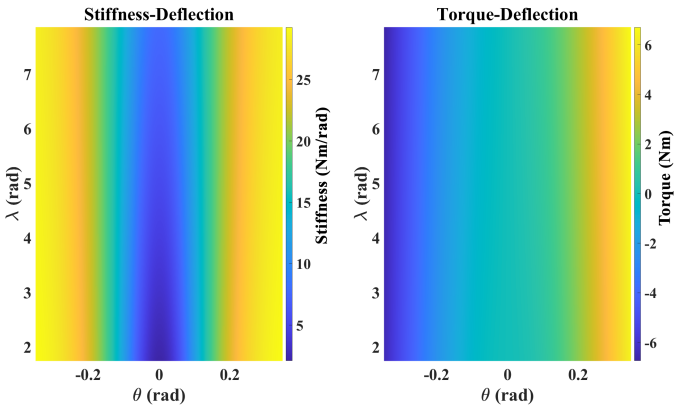

Fig. 4. The stiffness-deflection (left) and torque-deflection (right) relation from simulation for the inherent stiffness of springs, $k_s = 3300$ N/m.

C. Torque Estimation

1) Friction-Compensated Torque Estimation Model: An important advantage of elastic actuator is that the output torque can be estimated without additional torque/force sensors reducing the size, weight, and cost. Previous studies established torque estimation models based on the mechanical structure, which estimates the output torque with deflection angles and angular speed. Friction compensation is utilized to improve the estimation accuracy [10], [38], which is established based on the following assumption:

Assumption 3. *The friction is related to the rotational speed, ω_θ, between input and output rings, and it produces a resistance torque $\tau_f = k_f\omega_\theta$.*

Then, the estimated output torque of friction-compensated model can be found as

$$\begin{aligned} \tau_{o,f} &= \tau - \tau_f. \\ &= NF_{xy}r - k_f\omega_\theta \end{aligned} \tag{11}$$

where $\tau_{o,f}$ is the estimated output torque of the friction-compensated model. The value of k_f can be determined by minimizing the least-squared error between the estimated and the measured output torque.

2) Polynomial Torque Estimation Model: Besides the friction-compensated model, this study also establishes a polynomial model to estimate the output torque. By incorporating high-dimension factors and considering the non-linearity, the polynomial model surpassed the simplified assumptions of Hooke's law, resulting in better torque estimation. The polynomial model is defined as a 6^{th} degree polynomial model, which is written as

$$\begin{aligned} \tau_{o,p} =& p_0 + p_1\theta + p_2\lambda + p_3\omega_\theta + p_4\theta^2 + p_5\theta\lambda + \\ & p_6\theta\omega_\theta + p_7\lambda^2 + p_8\lambda\omega_\theta + p_9\omega_\theta^2 + \ldots + p_{84}\omega_\theta^6 \end{aligned} \tag{12}$$

where $\tau_{o,p}$ is estimated output torque of the polynomial model. The parameter matrix $P = \{p_0, p_1, p_2, ..., p_{84}\}$ is determined by minimizing the least-squared error between the estimated and measured output torque.

IV. Experiments Setup

To evaluate the performance of the proposed VSA, a test platform is build as shown in Fig. 5(a). The values of θ and λ are recorded by the encoders at a frequency of 1000 Hz. Kalman filters are implemented to reduce measurement noise in the deflection angles. ω_θ is obtained by applying a tracking-differentiator to the filtered deflection angles [42]. Additionally, the output torque of the actuator is monitored using a torque sensor, operating at a frequency of 250 Hz.

Five groups of test are carried out to evaluate the torque estimation models Eqns. 11 and 12 at three different λ, with $k_s = 3300$ N/m. PID controllers are developed to achieve the control of θ and λ. The control diagram is shown in Fig. 5(b).

V. Result

A. Torque Estimation

The deflection angle, θ is tested from θ_{min} to θ_{max} for three different spring preload conditions, set λ as $\lambda_1 = 50°$,

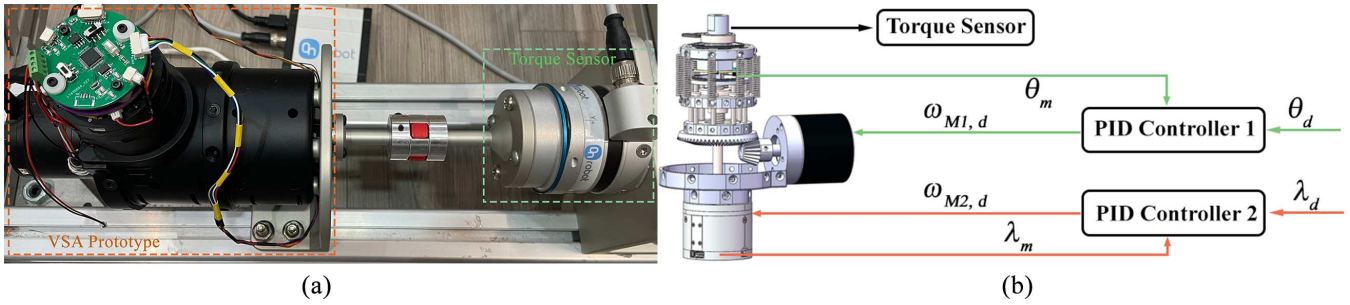

Fig. 5. (a) Experiment setup of the performance test; (b) The control diagram for the performance test. $\omega_{M1,d}$ and $\omega_{M2,d}$ are the desired speeds of M1 and M2, respectively. θ_m and θ_d are the measured and desired value of θ, λ_m and λ_d are the measured and desired value of λ

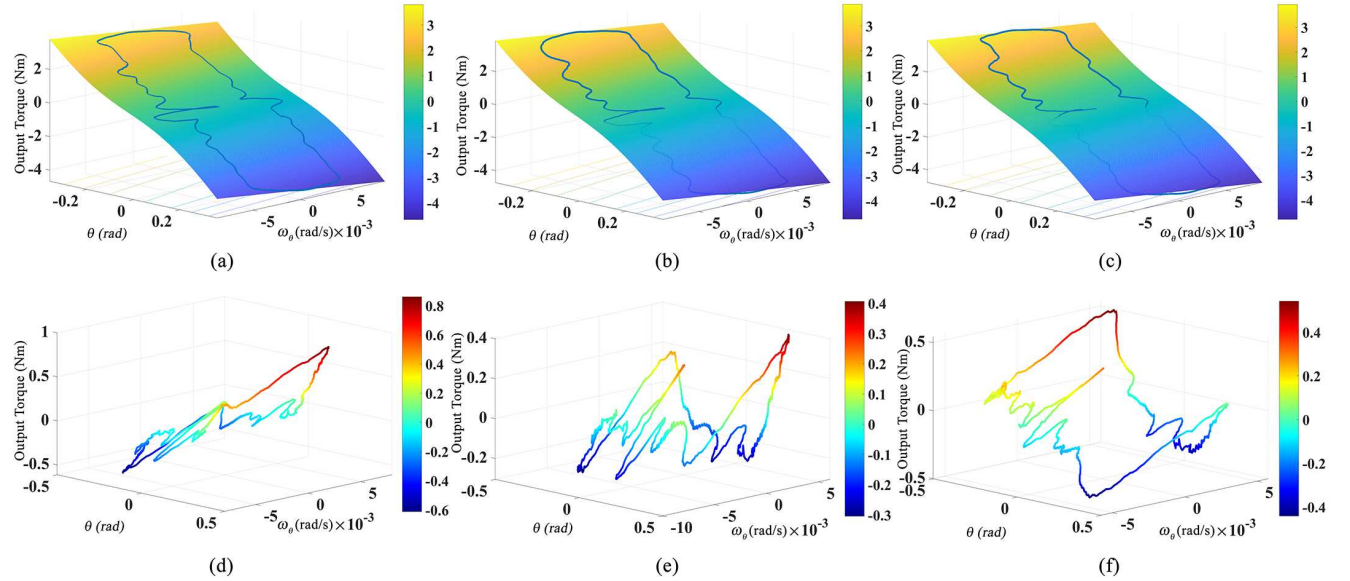

Fig. 6. (a), (b), and (c) show the comparison between output torque measured by the torque sensor and estimated by the friction-compensated model for $\lambda = \lambda_1$, λ_2 and λ_3, respectively. (d), (e), and (f) demonstrate the corresponding error between the estimated and measured output torque.

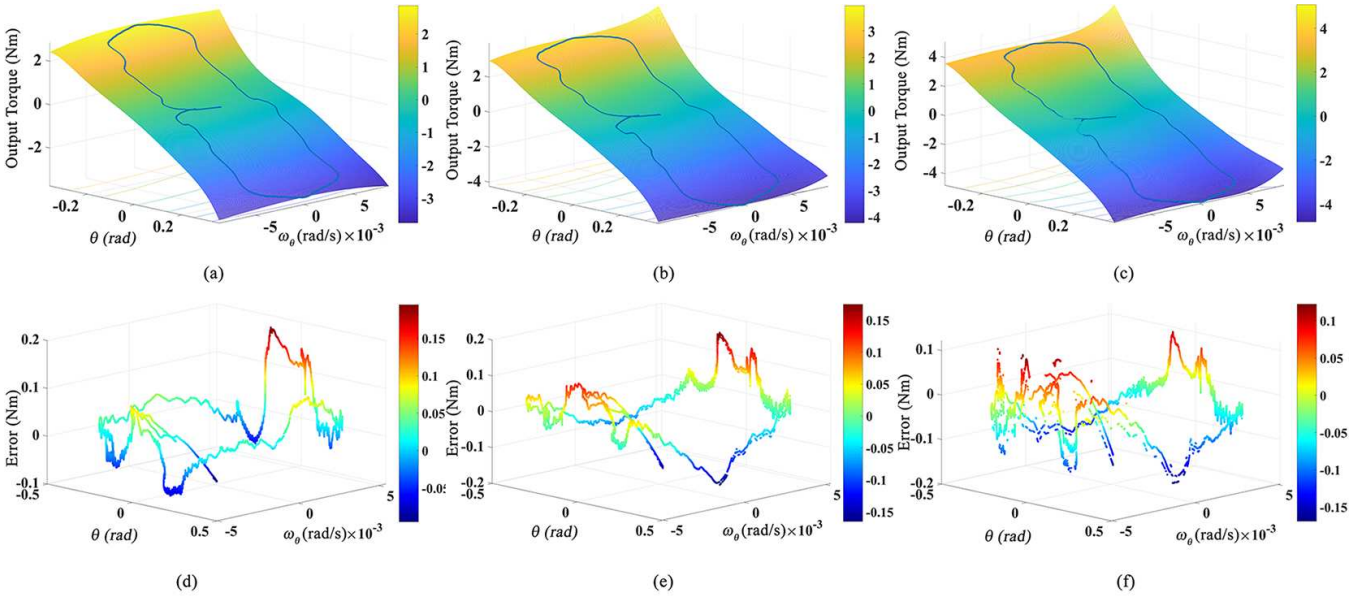

Fig. 7. (a), (b), and (c) show the comparison between the output torque measured by torque sensor and estimated by the polynomial model for $\lambda = \lambda_1$, λ_2 and λ_3, respectively. (d), (e), and (f) demonstrate the corresponding error between the estimated and measured torque.

TABLE I
COMPARISON OF THE OPERATING SPECIFICATIONS OF SERIAL VSAS.

Name	Mass (Kg)	Range of Stiffness (Nm/rad)	Stiffness Regulation Time (s)	Range of Motion (°)	Range of Deflection (°)	Nominal Torque (Nm)	Peak Torque (Nm)	Size (W×H×L) (mm)	Volume (10^{-3}/m^3)	Power (W)	PV (10^3/m^3)	PW (W/Kg)
TPS-VSA	**0.86**	**0∼rigid**	**0.9**	**±150**	**±30**	**6.0**	**20**	**90×95×126**	**2.01**	**200**	**99.50**	**232.56**
MACCEPA [23]	2.4	5∼110	2.6	±150	0∼60	50	70	-	4.80	200	41.67	83.33
AwAS-II [16], [17]	1.1	0∼rigid	0.8	±150	±17	10.75	80	130×270	3.43	56	16.33	50.91
RVSA [10]	2.0	3.5∼549	0.38	±135	±20	19	66.6	639×137×137	-	-	-	-
S^{3}VSA [24]	0.87	12.12∼rigid	0.1	0∼360	±12	7.56	22.7	125×125×118	2.24	200	89.29	229.89
LVSA [9]	0.41	0∼988	0.22	±180	±25	2.5	3.8	140×140×65	1.27	100	78.74	243.90

$\lambda_2 = 410°$ and $\lambda_3 = 770°$, respectively. During the test, θ, ω_θ and λ are recorded by the encoders. Output frame of the VSA is coupled with the torque sensor which monitors the output torque, and is fixed to the test bed. A set of data is utilized to identify the k_f of Eqn. (11), and P of Eqn. (12). The two estimation models are utilized to predict the output torque based on the deflection angles, and angular speed. Figs. 6 and 7 show the comparison between estimated and measured torque, and estimation error of the two models, respectively.

Root-mean-squared error ($RMSE$) is used to quantify estimation accuracy of the torque estimation models, which is defined as

$$RMSE = \sqrt{\frac{1}{N}\sum_{i=1}^{N}(\tau_i - \widehat{\tau}_i)^2} \tag{13}$$

where τ_i is the measured torque, and $\widehat{\tau}_i$ is the torque estimated by the model. Table. II summarizes the $RMSE$ values for both $\lambda = \lambda_1$, λ_2 and λ_3.

TABLE II
RMSE VALUES FOR QUANTIFY TORQUE ESTIMATION ACCURACY.

Model	$RMSE_{\tau,1}$(Nm)	$RMSE_{\tau,2}$(Nm)	$RMSE_{\tau,3}$(Nm)
Eqn. (12)	0.0663	0.0737	0.0580
Eqn. (11)	0.2933	0.1167	0.2279

B. Free Vibration Test

To explore and analyze the dynamic behavior of the actuator, free vibration tests are conducted for three different spring preload with a pendulum, i.e., $\lambda = \lambda_1$, λ_2 and λ_3, respectively. The pendulum is released from the initial position $\theta = 20.0°$, and the subsequent motion is captured by the encoders. Fig. 8 shows time history of the three tests, and the frequency responses obtained by Fast Fourier Transform (FFT).

C. Stiffness Regulation Test

Stiffness regulation test is performed to evaluate the speed that the VSA can adjust its stiffness, i.e., stiffness regulation time. During the test, the deflection angle, θ, is kept constant, and output torque of the VSA is recorded by a torque sensor to identify the change of stiffness. λ is set to change between its lower and upper boundaries to regulate the output stiffness. Fig. 9 illustrates the recorded change of θ, λ, output torque measured by the torque sensor, and the stiffness change estimated by Eqn. (10).

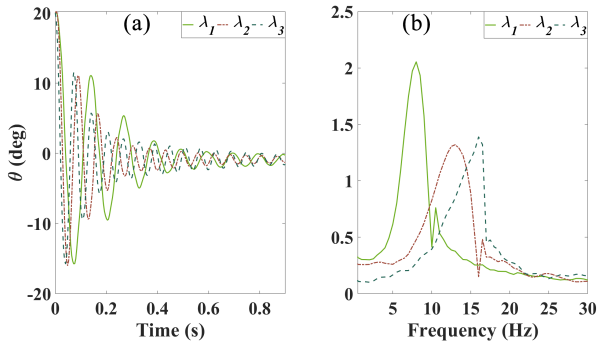

Fig. 8. (a) time history of θ of the free vibration; (b) frequency responses obtained from the test.

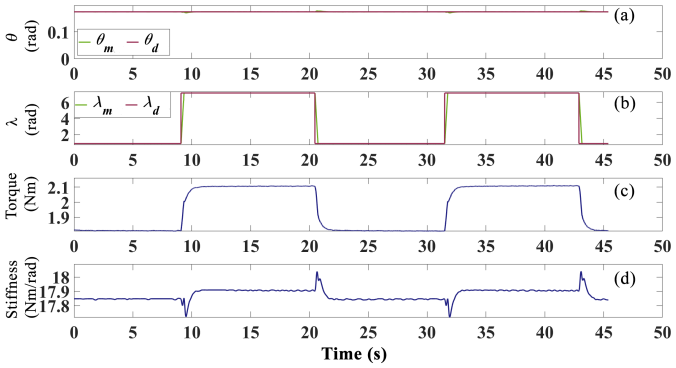

Fig. 9. Result of stiffness regulation test: (a) Time history of θ between the output and input rings, θ; (b) Deflection regulation of stiffness adjuster, λ; (c) Measured output torque during the stiffness regulation; (d) Stiffness change during the test.

D. Trajectory Tracking

Trajectory tracking test is carried out to demonstrate the tracking accuracy of the VSA with a basic position controller. The output frame of the actuator is coupled with a 1.5 kg load. Fig. 10(a) shows the setup of the tracking test.

The test involves three different sinusoidal reference trajectories. Fig. 10(b) shows comparison between the desired and recorded position of output frame of TPS-VSA during the tests. To quantify the tracking accuracy, RMSE values for all the tests are calculated and summarized in Table. III.

VI. DISCUSSION

The simulation result in Fig. 4 illustrates that the proposed actuator can produce a torque related to θ and λ, up to about

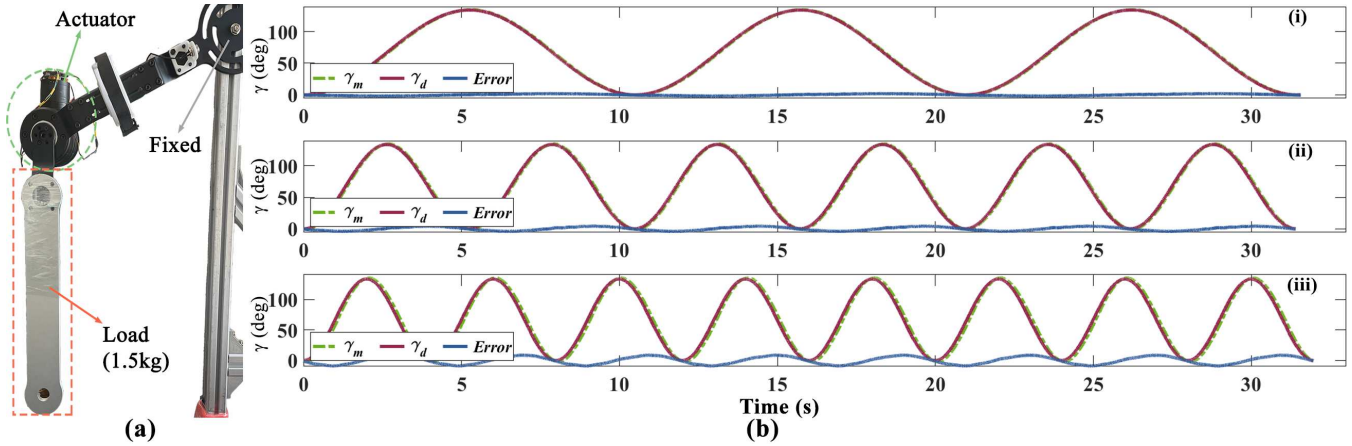

Fig. 10. (a) Experiment setup of the position tracking test; (b) illustrate the trajectory tracking result for the test conducted with three different sinusoidal desired trajectories. γ_m and γ_d are the measured and desired position of the output ring. $Error$ is the error between γ_m and γ_d.

TABLE III
RMSE VALUES FOR QUANTIFY TRAJECTORY TRACKING ACCURACY.

$RMSE_1$(deg)	$RMSE_2$(deg)	$RMSE_3$(deg)
1.2181	2.7858	6.0058

$RMSE_1$, $RMSE_2$ and $RMSE_3$ represent the tracking accuracy of the test shown in Fig. 10(b)-(i), (ii) and (iii), respectively.

6.0 Nm. It also shows the stiffness-deflection relation which indicates that the stiffness of the actuator can be adjusted through changing λ. This validates the proposed mechanism an effective way of stiffness variation for series VSAs.

Figs. 7 and 6, and Table. II show that both the polynomial and friction-compensated models can estimate the output torque of the VSA with good accuracy. However, it is clear that the average estimation accuracy, i.e., $RMSE$, of the polynomial model is significantly lower than that of the friction-compensated model. This indicates that there might be high-dimensional factors influencing the estimation result, thereby causing the polynomial model, with its higher complexity, to outperform the friction-compensated model. For example, the torsion deformation of spring leads to non-linearity in the spring force. To tackle this problem, the torque estimation model needs to consider the non-linearity or high-stiffness springs should be used to reduce torsion deformation by limiting θ. Although the polynomial model shows good performance in torque estimation, there are several issues in incorporating such a model into the controllers. Firstly, the computational cost of this model is much higher than that of the friction-compensated model as it involves many complex terms. Secondly, the first derivative of the polynomial model cannot be used to estimate the stiffness of the output frame, which means an additional model is required for stiffness estimation. Finally, considering angular speed can compensate for the non-linearity in the system, while this may bring challenges in torque control as it introduces an optimization problem, and it is difficult to control the deflection angle and the speed together with only one input. Additionally, for different λ, the maximal error of the polynomial model is about 2∼3 times to the average error, while the maximal error of the friction-compensated model reaches about 1 Nm which about 3∼8 times to the average error. This also validates that the polynomial model is more reliable than the friction-compensated model.

Fig. 8 demonstrates the dynamic behavior and frequency responses of the VSA in the free vibration test. As can be seen, the increase of λ increases the stiffness of the output frame of TPS-VSA, which is also validated by the change of natural frequency of the VSA with different λ, see Fig. 8 (b).

Table. I shows the comparison between the TPS-VSA and the typical actuators proposed by earlier studies. It is clear that the proposed weight and size of the proposed VSA is relatively lower and smaller, and with promising range of stiffness and output torque. However, the range of motion is relatively smaller than other actuators. The reason is that the off-axis encoder A is connected with output ring, thus the cables of encoder A restricted the movement of other components. This restriction can be completely removed by placing encoder A on the inner side of the external case of TPS-VSA to detect the absolute displacement of the input ring which can be defined as θ_{abs}. Therefore, θ can be obtained by calculating the difference between the absolute displacement of input and output rings, i.e., $\theta = \theta_{abs} - \gamma$.

As it is hard to measure the stiffness of output frame directly, a torque sensor is employed to monitor the output torque change during the test to validate the variation of stiffness. As shown in Fig. 9, the stiffness regulation time is about 0.9 s, which is relatively slow compared to other actuators listed in Table. I. Therefore, there is a need to improve the stiffness regulation speed in order to enhance the actuator's responsiveness to environmental changes. There are three different ways to achieve this: 1) using ball screw with larger lead length d, which will reduce the required deflection angle of stiffness regulation motor λ for same change of spring pre-compression Δh_2; 2) using shorter springs and increasing the radius of output ring, which, however, will reduce the range of deflection θ since the safe travel length of spring decreases with its length; 3) replacing the gear box of M2 with lower reduction ratio so that M2 can move the ball screw nut faster.

According to Eqn. (10), the stiffness-deflection profile of the

TPS-VSA is nonlinear. Therefore, achieving linear stiffness tracking control in practice poses a challenge. One effective approach is to develop an accurate real-time stiffness estimation model and implement an advanced controller, such as adaptive control or model predictive control, to compensate for the nonlinearity. Additionally, increasing the speed of M2 is recommended to reduce mechanical stiffness regulation time, which can enhance the stiffness compensation performance. Finally, if the desired stiffness $k_{eq,d}$ is lower than the real-time stiffness k_{eq}, it is possible to emulate $k_{eq,d}$ using algorithms. This can serve as a complementary stiffness regulation method alongside mechanical adjustments.

Trajectory tracking result shown in Fig. 10(b) demonstrates that the TPS-VSA with a basic position controller can track different reference trajectories with good accuracy, see Table. III. However, the tracking error increases with the frequency of the sinusoidal reference trajectory obviously. To solve this, the spring stiffness should be increased to expand the bandwidth of the actuator. Also, the position controller needs to be further improved by adding more feedback, such as angular speed, and acceleration.

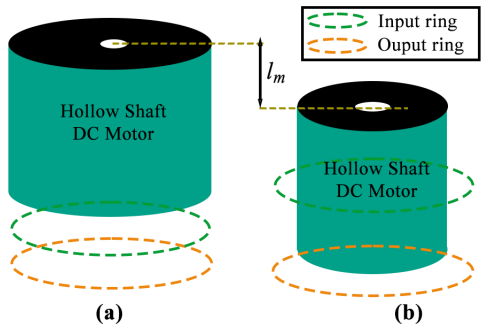

Fig. 11. Illustration of two solutions to optimize the structure of TPS-VSA. The input and output rings are coupled with parallel springs for both solutions.

Finally, the presented design of the Variable Stiffness Actuator (VSA) can still be optimized to reduce size and weight. For instance, the input ring can be directly driven by a hollow shaft DC motor, eliminating the need for bevel gears and M1, resulting in a significant reduction in dimensions and increased power transmission efficiency. Figure 11 illustrates two potential solutions for optimizing the actuator's structure by replacing M1 with a hollow shaft DC motor. In solution (a), the DC motor is positioned on top of the input ring. In solution (b), the DC motor is placed below the input ring to reduce the overall height of the actuator. If the radius of the input ring is the same in both solutions (a) and (b), solution (b) typically requires a smaller radius for the DC motor. In other words, the actuator's capability can be enhanced by increasing the radius of the input ring in solution (b). Furthermore, as per Equation 7, the ratio r_2/l_0 can be further optimized to achieve comparable performance with a smaller size and lighter weight. However, this optimization necessitates a balance between the output capacity and the deflection range, considering that the maximum safe travel length of a spring decreases with its original length.

VII. CONCLUSIONS AND FUTURE WORK

This study proposes a novel twisting mechanism with parallel springs, named TPS, for series VSAs, which enables the optimization of the structure and size of VSAs. A series VSA is designed based on the TPS mechanism and evaluated with a prototype, TPS-VSA. The stiffness and output capacity of the design are analyzed through simulation. A friction-compensated model and a polynomial model are established to estimate the output torque of TPS-VSA based on the deflection angles and angular speed. The accuracy of both models is validated through experiments by comparing their torque estimations with measurements from the torque sensor. The results illustrate that both models can estimate the output torque accurately, but the estimation error of the polynomial model is lower than 0.0737 Nm, significantly outperforming the friction-compensated model, see Table II. The dynamic behavior and frequency responses of TPS-VSA demonstrate that the proposed mechanism can effectively regulate the stiffness, which is also validated by the stiffness regulation test. Finally, the trajectory tracking result indicates that the actuator can accurately track different trajectories with the controller. However, our study also reveals several limitations of TPS-VSA: 1) The torsion deformation of springs introduces non-linearity in torque estimation, limiting torque estimation accuracy. 2) The trajectory tracking ability of TPS-VSA is limited. 3) The values of r_2 and l_0 need to be further optimized to increase the output capacity and reduce the weight and size. Further work will involve exploring better dimensions of the mechanical components to optimize the performance of TPS-VSA, incorporating angular speed and acceleration feedback to improve controller performance, and incorporating non-linear compensatory terms to enhance torque estimation accuracy.

REFERENCES

[1] A. Calanca and P. Fiorini, "On the Role of Compliance in Force Control," *Intelligent Autonomous Systems 13*, pp. 1243-1255, 2015.
[2] N. Hogan, "Contact and physical interaction," *Annu. Rev. Control Rob. Auton. Syst.*, vol. 5, no. 1, pp. 179–203, 2022.
[3] W. Zhao, J. Liao, W. Qian, H. Yu, and Z. Guo, "A novel design of series elastic actuator using Tensile Springs Array," *Mech. Mach. Theory*, vol. 192, p. 105541, 2024.
[4] B. Zhong, K. Guo, H. Yu, and M. Zhang, "Toward gait symmetry enhancement via a cable-driven exoskeleton powered by series Elastic Actuators," *IEEE Rob. Autom. Lett.*, vol. 7, no. 2, pp. 786–793, 2022.
[5] E. Capotorti, E. Trigili, Z. McKinney, E. Peperoni, F. Dell'Agnello, M. Fantozzi, A. Baldoni, D. Marconi, E. Taglione, S. Crea, and N. Vitiello, "A novel torque-controlled hand exoskeleton to decode hand movements combining SEMG and fingers kinematics: A feasibility study," *IEEE Rob. Autom. Lett.*, vol. 7, no. 1, pp. 239–246, 2022.
[6] T. Kim, K. Shi, and K. Kong, "A compact transmitted-force-sensing series elastic actuator with optimized planar torsional spring for exoskeletons," *2021 IEEE/ASME International Conference on Advanced Intelligent Mechatronics (AIM)*, 2021.
[7] G. Raiola, C. A. Cardenas, T. S. Tadele, T. de Vries and S. Stramigioli, "Development of a Safety- and Energy-Aware Impedance Controller for Collaborative Robots," *IEEE Rob. Autom. Lett.*, vol. 3, no. 2, pp. 1237-1244, April 2018.
[8] Z. Li, W. Chen and S. Bai, "A Novel Reconfigurable Revolute Joint with Adjustable Stiffness," *2019 International Conference on Robotics and Automation (ICRA)*, Montreal, QC, Canada, 2019, pp. 8388-8393.
[9] C. Wang et al., "A lightweight series elastic actuator with variable stiffness: Design, modeling, and evaluation," *IEEE/ASME Trans. Mechatron.*, pp. 1–10, 2023.

[10] Y. Zhu, Q. Wu, B. Chen, D. Xu and Z. Shao, "Design and Evaluation of a Novel Torque-Controllable Variable Stiffness Actuator With Reconfigurability," *IEEE/ASME Trans. Mechatron.*, vol. 27, no. 1, pp. 292-303, 2022.

[11] R. Mengacci, M. Keppler, M. Pfanne, A. Bicchi, and C. Ott, "Elastic structure preserving control for compliant robots driven by agonistic-antagonistic actuators (ESPAA)," *IEEE Rob. Autom. Lett.*, vol. 6, no. 2, pp. 879–886, 2021.

[12] W. Roozing, Z. Li, G. A. Medrano-Cerda, D. G. Caldwell, and N. G. Tsagarakis, "Development and control of a compliant asymmetric antagonistic actuator for Energy Efficient Mobility," *IEEE/ASME Trans. Mechatron.*, vol. 21, no. 2, pp. 1080–1091, 2016.

[13] T. Luong, S. Seo, K. Kim, J. Jeon, F. Yumbla, J. C. Koo, H. R. Choi, and H. Moon, "Realization of a simultaneous position-stiffness controllable antagonistic joint driven by twisted-coiled polymer actuators using model predictive control," *IEEE Access*, vol. 9, pp. 26071–26082, 2021.

[14] C. W. Mathews and D. J. Braun, "Design of parallel variable stiffness actuators," *IEEE Trans. Rob.*, vol. 39, no. 1, pp. 768–782, 2023.

[15] W. Roozing, Z. Ren, and N. G. Tsagarakis, "An efficient leg with series–parallel and BIARTICULAR compliant actuation: Design optimization, modeling, and control of the eleg," *Int. J. Rob. Res.*, vol. 40, no. 1, pp. 37–54, 2019.

[16] A. Jafari, N. G. Tsagarakis, B. Vanderborght, and D. G. Caldwell, "A novel actuator with adjustable stiffness (AWAS)," *2010 IEEE/RSJ International Conference on Intelligent Robots and Systems*, 2010.

[17] A. Jafari, N. Tsagarakis and D. Caldwell, "AwAS-II: A new Actuator with Adjustable Stiffness based on the novel principle of adaptable pivot point and variable lever ratio," *2011 IEEE International Conference on Robotics and Automation*, 2011.

[18] E. Sariyildiz, R. Mutlu, J. Roberts, C.-H. Kuo, and B. Ugurlu, "Design and control of a novel variable stiffness series elastic actuator," *IEEE/ASME Trans. Mechatron.*, pp. 1–12, 2023.

[19] S. Wolf, G. Grioli, O. Eiberger, W. Friedl, M. Grebenstein, H. Hoppner, E. Burdet, D. G. Caldwell, R. Carloni, M. G. Catalano, D. Lefeber, S. Stramigioli, N. Tsagarakis, M. Van Damme, R. Van Ham, B. Vanderborght, L. C. Visser, A. Bicchi, and A. Albu-Schaffer, "Variable stiffness actuators: Review on design and components," *IEEE/ASME Trans. Mechatron.*, vol. 21, no. 5, pp. 2418–2430, 2016.

[20] J. Sun, Z. Guo, D. Sun, S. He, and X. Xiao, "Design, modeling and control of a novel compact, energy-efficient, and rotational serial variable stiffness actuator (SVSA-II)," *Mech. Mach. Theory*, vol. 130, pp. 123–136, 2018.

[21] N. G. Tsagarakis, I. Sardellitti, and D. G. Caldwell, "A new variable stiffness actuator (compact-VSA): Design and modelling," *2011 IEEE/RSJ International Conference on Intelligent Robots and Systems*, 2011.

[22] Y. Liu, S. Cui, and Y. Sun, "Mechanical design and analysis of a novel variable stiffness actuator with symmetrical pivot adjustment," *Front. Mech. Eng.*, vol. 16, no. 4, pp. 711–725, 2021.

[23] B. Vanderborght, N. G. Tsagarakis, C. Semini, R. Van Ham and D. G. Caldwell, "MACCEPA 2.0: Adjustable compliant actuator with stiffening characteristic for energy efficient hopping," *2009 IEEE International Conference on Robotics and Automation*, 2009.

[24] Y. Xu, K. Guo, J. Sun, and J. Li, "Design, modeling and control of a reconfigurable variable stiffness actuator," *Mech. Syst. Signal Process.*, vol. 160, p. 107883, 2021.

[25] Y. Xu, K. Guo, J. Li, and Y. Li, "A novel rotational actuator with variable stiffness using S-shaped springs," *IEEE/ASME Trans. Mechatron.*, vol. 26, no. 4, pp. 2249–2260, 2021.

[26] L. Miskovic, M. Dezman, and T. Petric, "Pneumatic quasi-passive variable stiffness mechanism for energy storage applications," *IEEE Rob. Autom. Lett.*, vol. 7, no. 2, pp. 1705–1712, 2022.

[27] Y. Sun, P. Tang, D. Dong, J. Zheng, X. Chen, and L. Bai, "Modeling and experimental evaluation of a pneumatic variable stiffness actuator," *IEEE/ASME Trans. Mechatron.*, vol. 27, no. 5, pp. 2462–2473, 2022.

[28] B. H. Do, I. Choi, and S. Follmer, "An all-soft variable impedance actuator enabled by embedded layer jamming," *IEEE/ASME Trans. Mechatron.*, vol. 27, no. 6, pp. 5529–5540, 2022.

[29] Y. Feng et al., "Safety-enhanced control strategy of a power soft robot driven by hydraulic artificial muscles," *ROBOMECH J.*, vol. 8, no. 1, 2021.

[30] M. Sun, X. Ouyang, J. Mattila, Z. Chen, H. Yang and H. Liu, "Lightweight electrohydrostatic actuator drive solution for Exoskeleton Robots," *IEEE/ASME Trans. Mechatron.*, vol. 27, no. 6, pp. 4631–4642, 2022.

[31] E. Barrett, J. Malzahn, and N. Tsagarakis, "A compliant mechanism with progressive stiffness for robotic actuation," *2021 IEEE/ASME International Conference on Advanced Intelligent Mechatronics (AIM)*, 2021.

[32] X. Li, H. Zhu, W. Lin, W. Chen and K. Low, "Structure-Controlled Variable Stiffness Robotic Joint Based on Multiple Rotary Flexure Hinges," *IEEE Trans. Ind. Electron.*, vol. 68, no. 12, pp. 12452-12461, 2021.

[33] R. Chaichaowarat, S. Nishimura, and H. I. Krebs, "Design and modeling of a variable-stiffness spring mechanism for impedance modulation in physical human–robot interaction," *2021 IEEE International Conference on Robotics and Automation (ICRA)*, 2021.

[34] J. Sun, Z. Guo, Y. Zhang, X. Xiao and J. Tan, "A Novel Design of Serial Variable Stiffness Actuator Based on an Archimedean Spiral Relocation Mechanism," *IEEE/ASME Trans. Mechatron.*, vol. 23, no. 5, pp. 2121-2131, 2018.

[35] K. W. Hollander, T. G. Sugar and D. E. Herring, "Adjustable robotic tendon using a 'Jack Spring'," *9th International Conference on Rehabilitation Robotics*, 2005. pp. 113-118.

[36] Z. Li, W. Chen, J. Zhang, Q. Li, J. Wang, Z. Fang, and G. Yang, "A novel cable-driven antagonistic joint designed with variable stiffness mechanisms," *Mech. Mach. Theory*, vol. 171, p. 104716, 2022.

[37] Z. Liu, H. Jin, H. Zhang, Y. Liu, Y. Long, X. Liu, and J. Zhao, "A variable stiffness actuator based on second-order lever mechanism and its manipulator integration," *2021 IEEE International Conference on Robotics and Automation (ICRA)*, 2021.

[38] Y. F. Liu et al., "Modeling and control of piezoelectric inertia–friction actuators: Review and Future Research Directions," *Mech. Sci.*, vol. 6, no. 2, pp. 95–107, 2015.

[39] L. Deng et al., "Investigation of a seat suspension installed with compact variable stiffness and damping rotary magnetorheological dampers," *Mechanical Systems and Signal Processing*, vol. 171, p. 108802, 2022.

[40] L. Deng et al., "Innovative variable stiffness and variable damping magnetorheological actuation system for robotic arm positioning," *Journal of Intelligent Material Systems and Structures*, vol. 34, no. 2, pp. 123–137, 2022.

[41] L. Deng et al., "A new magnetorheological quasi-zero stiffness vibration isolation system with large zero stiffness range and highly stable characteristics," *Nonlinear Dynamics*, 2023.

[42] B.-Z. Guo, J.-Q. Han, and F.-B. Xi, "Linear tracking-differentiator and application to online estimation of the frequency of a sinusoidal signal with random noise perturbation," *Int. J. Syst. Sci.*, vol. 33, no. 5, pp. 351–358, 2002.

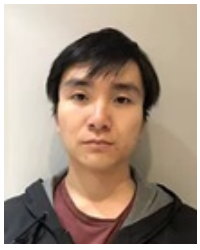

Chao Wang received the B.Eng. degree in electrical engineering from the Zhengzhou University, Henan, China, in 2017. He is currently pursuing the Ph.D. degree in the mechatronics with the School of Electronic and Electrical Engineering, University of Leeds, Leeds, U.K.

His research interests include human-robot interaction, compliant actuation systems and rehabilitation robotics.

Zhenhong Li (Member, IEEE) received a BEng degree in electrical engineering from Huazhong University of Science and Technology, China, and MS and PhD degrees in control engineering from the University of Manchester, U.K., in 2014 and 2019, respectively. From 2019-2023, he was a research fellow in rehabilitation robotics at the University of Leeds, U.K. Since 2023, he has been a Lecturer in robotics and control with the University of Manchester.

His research interests include cooperative control of multi-agent systems and physical human-robot interactions.

Bo Sheng (Member, IEEE) received the M.Eng. degree in mechatronics from the Huazhong University of Science and Technology, Wuhan, China, in 2014, and the Ph.D. degree in mechanical engineering from the University of Auckland, Auckland, New Zealand, in 2019.

From 2019 to 2021, he was a Research Associate with the Department of Exercise Sciences, University of Auckland. He is currently a Lecturer with the School of Mechatronic Engineering and Automation, Shanghai University, Shanghai, China. He has participated in more than ten research projects in areas of rehabilitation robots, interaction control, and medical informatics. He is the author of more than 26 academic journal and conference papers. His research interests include robot-assisted rehabilitation, human–robot interaction, and medical informatics.

Tianzhe Bao received the BS and MS degrees in traffic and transportation engineering from Central South University, Changsha, China, in 2014 and 2017, respectively, and PhD degree in electronic and electrical engineering from University of Leeds, Leeds, UK. He is currently an assistant professor in University of Health and Rehabilitation Sciences, Qingdao, China.

His research interests include sEMG signals processing, myoelectric control, machine learning, and deep learning.

Manoj Sivan received the M.D. degree from University of Leeds, Leeds, U.K., in 2014. He is an Associate Clinical Professor and Honorary Consultant in Rehabilitation Medicine (RM) with University of Leeds and Leeds NHS Trusts. He received the prestigious European Academy and Philip Nichols awards in 2014 for his research in upper limb rehabilitation robotics. His Covid rehabilitation work won his team the 2021 BMJ Clinical Leadership Team award and the digital application C19-YRS system he helped develop won the 2021 Medipex NHS Innovation award. He is an advisor for the World Health Organisation (WHO) for its Covid rehabilitation policy in Europe.

His research interests are rehabilitation technology, health services, upper limb rehabilitation, chronic pain, and outcome measurement. His work is supported by research grants from NIHR, MRC, EPSRC, ISRT, Research England and RCP. He is the Editor-in-Chief (EIC) for the journal Rehabilitation Process and Outcome and the EIC for the Oxford Handbook of Rehabilitation Medicine.

Zhiqiang Zhang (Member, IEEE) received the Ph.D. degree in electrical engineering from the University of Chinese Academy of Sciences, Beijing, China, in 2010. He was a research associate in Imperial College London for five and half years. He is an Associate Professor in body sensor networks for healthcare and robotic control with the University of Leeds, Leeds, U.K. He has more than 50 papers in peer-reviewed publications.

His research interests are human kinematics, musculoskeletal modeling, and machine learning.

Guqiang Li received the M.Sc. degree in sport body science from the Jiangsu Normal University, Xuzhou, China, in 2008.

He is currently an Associate Professor with the School of Rehabilitation Medicine, Binzhou Medical University, Yantai, China. His research interests include rehabilitation robotics, intelligent rehabilitation assistive devices, and 3D-printed orthosis in the clinic.

Sheng Quan Xie (Fellow, IEEE) received the Ph.D. degree in mechanical engineering from the University of Canterbury, Christchurch, New Zealand, in 2002. In 2003, he joined the University of Auckland and became a Chair Professor in (Bio) mechatronics in 2011. Since 2017, he has been the Chair of Robotics and Autonomous Systems with the University of Leeds, Leeds, U.K. He has authored or coauthored eight books, 15 book chapters, and more than 400 international journal and conference papers. His current research interests include medical and rehabilitation robots and advanced robot control.

Dr. Xie is an Elected Fellow of The Institution of Professional Engineers New Zealand.